Finite-temperature properties of the two-dimensional SU(2) Kondo necklace

Wolfram Brenig
Technische Universität Braunschweig, Mendelssohnstr. 3, 38106 Braunschweig, Germany
(Received 9 November 2005; published 30 March 2006)

We analyze several thermodynamic properties of the two-dimensional Kondo necklace using finite-temperature stochastic series expansion. In agreement with previous zero-temperature findings the model is shown to exhibit a quantum critical point (QCP), separating an antiferromagnetic from a paramagnetic dimerized state at a critical Kondo exchange-coupling strength $J_c \approx 1.4$. We evaluate the temperature dependent uniform and staggered structure factors as well as the uniform and staggered susceptibilities and the local "impurity" susceptibility close to the QCP as well as in the ordered and quantum disordered phase. The crossover between the classical, renormalized classical, and quantum critical regime is analyzed as a function of temperature and Kondo coupling.

DOI: 10.1103/PhysRevB.73.104450 PACS number(s): 75.10.Jm, 05.70.Jk, 75.40.Cx, 75.40.Mg

There is growing evidence that unconventional finite temperature properties of many novel materials stem from zero-temperature phase transitions, i.e., changes of the ground state symmetry as a function of some control parameter. Prominent potential candidates to show such quantum phase transitions are the cuprate superconductors,[1,2] quantum magnets,[3,4] and heavy-fermion or dense Kondo systems.[5,6] In the latter, quantum critical points (QCPs) can arise from the competition between magnetic long-range ordered (LRO) and renormalized paramagnetic metallic or semimetallic phases resulting from local Kondo screening. This has been conjectured early on by Doniach.[7] Semimetallic behavior in nonmagnetic states of Kondo lattice materials is typical for stoichiometric "Kondo insulators" like $CeNi_{1-x}Pt_xSn$ which undergoes a para-to-antiferromagnetic transition at $x \approx 0.2 \ldots 0.3$.[8,9] A model for such materials is the Kondo-Hubbard lattice model (KHLM)

$$H_{KH} = -t \sum_{lm,\sigma} c^{\dagger}_{l\sigma} c_{m\sigma} + U \sum_{l} n_{l\uparrow} n_{l\downarrow} + J \sum_{l,\alpha\beta} \mathbf{S}_{Pl} \cdot \mathbf{S}_{Il} \qquad (1)$$

with conduction electrons $c^{(\dagger)}_{l\sigma}$ of spin $\mathbf{S}_{Pl}$, which are correlated via an on-site Coulomb repulsion U, and coupled by antiferromagnetic (AFM) Kondo exchange to localized spins $\mathbf{S}_{Il}$ at sites l. At half filling on bipartite lattices in $D \geqslant 2$ dimensions and in the strong-coupling limit $U/t \gg 1$ the KHLM shows AFM LRO if the conduction-electron superexchange $j \sim t^2/U$ dominates the Kondo scale $T_K \sim t \exp \times(-1/\rho J)$ where ρ refers to the density of states (DOS).[10] Kondo screening will prevail if $T_K/j \gg 1$. On 2D square lattices the critical coupling $j_c(U/t)$ has been determined at temperature $T=0$ using projector QMC (Ref. 11) and bond-operator methods.[12] In the strong coupling limit and at half filling Eq. (1) simplifies to the SU (2)-symmetric so-called Kondo necklace (SKN)

$$H_{SKN} = j \sum_{lm} \mathbf{S}_{Pl} \cdot \mathbf{S}_{Pm} + J \sum_{l} \mathbf{S}_{Pl} \cdot \mathbf{S}_{Il} \qquad (2)$$

with $j \equiv 1$ hereafter. In this work we will focus on the two-dimensional (2D) square lattice, where at $T=0$ the SKN has been investigated by bond-operator methods, series expansion, and exact diagonalization.[13–15] These studies located a QCP at $J_c \sim 1.370 \ldots 1.408$ separating AFM LRO from a gapped spin-dimer phase. The latter can be viewed as the strong-coupling analog of the Kondo-screened paramagnetic state of the KHLM.

While the ground state properties of the 2D SKN have been studied rather extensively, thermodynamic and finite temperature critical properties of the SKN remain an open issue. Therefore, the aim of this work is to shed light on the 2D SKN at finite temperatures using a quantum Monte Carlo (QMC) approach. To this end we employ the stochastic series expansion (SSE) with loop updates introduced by Sandvik and Syljuasen in Refs. 16 and 17 to which we refer the reader for details on this approach.

We start by discussing the longitudinal staggered structure factor

$$S_n(\mathbf{Q}) = \langle (m^z_{n\mathbf{Q}})^2 \rangle, \qquad (3)$$

where $m^z_{n\mathbf{Q}} = \Sigma_l S^z_{nl} \exp(i\mathbf{Q} \cdot \mathbf{r}_l)/N_n$ is the staggered magnetization with $\mathbf{Q} = (\pi, \pi, \pi)$. $m^z_{n\mathbf{Q}}$ selects between $n = P, I, A$, for which $\mathbf{r}_l$ runs over the "conduction electron plane" for $n = P$, the "Kondo sites" for $n = I$, and all sites for $n = A$. Figure 1 shows the squared staggered moment $M^2_{\mathbf{Q}} = 3S_n(\mathbf{Q})$ vs J at low temperatures. The system sizes N_A are $L \times L \times 2 \equiv N$ with periodic boundary conditions (PBC) in the planar directions and $L = 24$ and 34. In all three panels $M^2_{\mathbf{Q}}$ is finite below a critical value of $J = J_c$ and drops to approximately zero for $J > J_c$. We identify J_c with the QCP and expect AFM LRO for $J < J_c$ in the thermodynamic limit at $T=0$. For $J > J_c$ we find no other transitions, i.e., the systems connect adiabatically to the limit of $J = \infty$. Therefore, it is dimerized. At fixed N, $M^2_{\mathbf{Q}}$ will saturate for $T \to 0$ due to finite size gaps. For $L = 24$ this is the case in Fig. 1(b) for $J \gtrsim 1$. Figure 1 allows no conclusion about the magnitude of the $T=0$ order parameter, which requires finite size scaling analysis.[18] The critical coupling, however, can be extracted efficiently from these results since J_c is almost invariant to increasing N or lowering T relative to the parameters in Fig. 1. To determine J_c we fit $M^2_{\mathbf{Q}}$ to a power law $M^2_{\mathbf{Q}} \approx c[J_c - J]^{\nu}$ in its region of negative curvature and for $J \gtrsim 1$. This procedure depends only little on

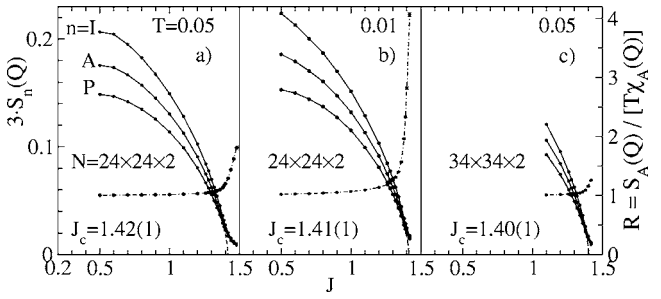

FIG. 1. Solid: staggered structure factor $S_n(\mathbf{Q})$ vs J close to the QCP at low-temperatures and for two system sizes: (a) $T=0.05$, $L=24$, (b) $T=0.01$, $L=24$, and (c) $T=0.05$, $L=34$. Dashed: fits of $S_P(\mathbf{Q})$ to $c[J_c-J]^\nu$ for $J\gtrsim 1$ with J_c indicated per panel. The fits depart visibly from $S_P(\mathbf{Q})$ only close to $J\approx 1.4$. Dashed-dotted: ratio of total staggered structure factor to susceptibility times T. If not indicated, statistical errors are less than the solid-circle marker size.

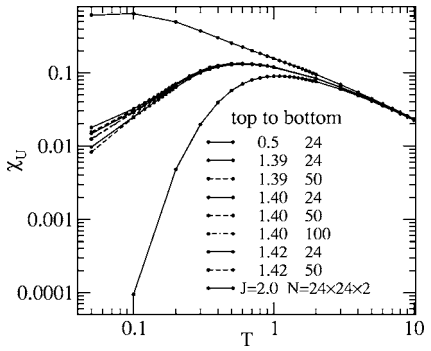

FIG. 2. Uniform susceptibility χ_u vs temperature for $0.05\leqslant T\leqslant 10$ and $0.5\leqslant J\leqslant 2.0$ at $L=24$ (solid) and for $1.39\leqslant J\leqslant 1.42$ at $L=50$ (100) [dashed(dashed-dotted)]. Statistical errors are less than the solid-circle marker size. The difference between $L=50$ and 100 at $J=1.40$ remains below the statistical error for all T depicted. Legends label plots from top to bottom.

the interval of J fitted to. The resulting scatter of J_c is taken to be a measure of the error and is displayed in Figs. 1(a)–1(c). We find that $J_c\approx 1.41(2)$. This agrees with $J_c\approx 1.41(1.39)$ from $T=0$ series expansion[13,14] and is also close to $J_c\approx 1.37$ from bond-operator Brückner theory.[14,19] A critical value of $J_c\approx 1.4(4t^2/U)$ is also consistent with projector-QMC at $T=0$ for the KHLM.[11]

For small J, $S_n(\mathbf{Q})$ remains strongly temperature dependent down to $T\ll 1$ which is due to the near decoupling of the I sites from the planar sites leading to a Curie-like contribution which is cutoff only at very low T. This is visible already at $J\lesssim 0.6$, by comparing $S_I(\mathbf{Q})$ in panels (a) and (b) of Fig. 1.

In addition to $S_n(\mathbf{Q})$ Fig. 1 includes results for the longitudinal staggered susceptibility

$$\chi_n(\mathbf{Q})=\int_0^\beta d\tau\langle m^z_{n\mathbf{Q}}(\tau)m^z_{n\mathbf{Q}}\rangle \tag{4}$$

for $n=A$ which have been encapsulated in the ratio

$$R=\frac{S_A(\mathbf{Q})}{T\chi_A(\mathbf{Q})}. \tag{5}$$

This ratio relates the analysis of $\chi_A(\mathbf{Q})$ to that of the AFM nonlinear σ model (NLσM).[20–22] From there it is expected that in the classical high-T, as well as in the low-T renormalized classical regime $R=1$, while $R\neq 1$ in the quantum critical regime. While this is consistent with $R(J)$ in Fig. 1, we will clarify later that the deviations of R from unity for $J\approx J_c$ are strongly affected by finite size effects.

Next we discuss the uniform susceptibility

$$\chi_u=\beta\langle m^2\rangle, \tag{6}$$

where $m=\Sigma_l S^z_{Al}/N_A$ is the total magnetization. In contrast to Eq. (4), the uniform susceptibility reduces to a simple expectation value, since $[H_{SKN},m]=0$. Figure 2 is a log-log plot of the dependence of χ_u on temperature over more than two decades $0.05\leqslant T\leqslant 10$ and for $0.5\leqslant J\leqslant 2$ with system sizes $L=24$, 50, and 100. For $T\geqslant 0.1$ finite-size effects are negligible if $L\geqslant 24$. For $0.05\leqslant T\leqslant 0.1$ finite-size effects, albeit small, have been considered for J in the vicinity of the QCP. As can be seen from the near identity of results with $L=50$ and 100 at $J=1.40$ in Fig. 2, it is sufficient to choose $L\gtrsim 50$ to reach the thermodynamic limit for all temperatures studied. For $T\gtrsim 2$ the uniform susceptibility turns Curie-like, independent of J. For $J>J_c$ the spin spectrum develops a gap Δ which implies a low-temperature behavior $\chi_u\propto\exp\times(-\beta\Delta)$. This is consistent with Fig. 2, where to within statistical error $\chi_u(T=0.05,J=2)=0$. For $0<J<J_c$ AFM LRO occurs at $T=0$, which agrees with the saturation of $\chi_u(T\to 0)=\chi_u^0$ shown in the figure. We note that as J vanishes χ_u^0 will diverge due to the Curie contribution from the impurity spins.

At the QCP we expect scaling of the uniform susceptibility. Indeed, for $J\approx J_c$, and at low temperatures χ_u follows nearly straight lines in Fig. 2. A close-up of this low-T region, shown in Fig. 3, evidences a weak curvature of $\chi_u(T)$ independent of the system size. These results allow excellent

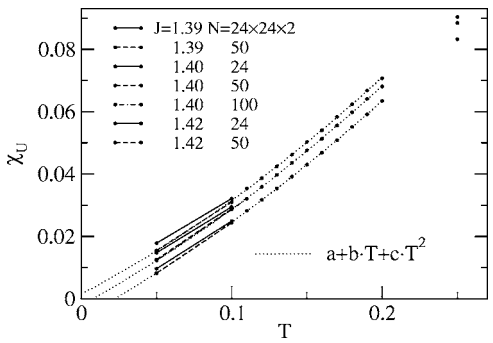

FIG. 3. Low-temperature uniform susceptibility $\chi_u(T)$ close to the QCP for $J=1.39$, 1.40, and 1.42 (from top to bottom). Dotted curves: fits of $\chi_u(T)$ to $a+bT+cT^2$. System sizes $L=24$ (solid), 50 (dashed), 100 (dashed-dotted) are indicated for $T\leqslant 0.1$. Statistical errors are less than the solid circle marker size. For $T\geqslant 0.11$ finite size effects are below statistical error and results for $J=1.40(1.39,1.42)$ refer to $L=100(24)$ only. The difference between $L=50$ and 100 at $J=1.40$ remains below the statistical error for all T depicted.

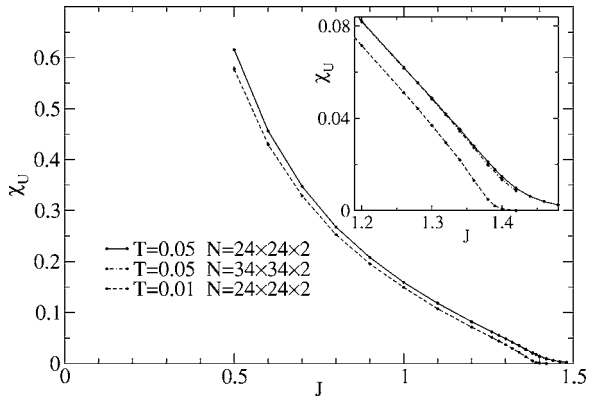

FIG. 4. Uniform susceptibility χ_u vs J on approaching the QCP for two temperatures $T=0.05(0.01)$ [solid(dashed) line] at fixed $L=24$, and comparing two system sizes $L=24(34)$ [solid(dashed-dotted) line] at fixed $T=0.05$. Finite size effects are exceedingly small and are shown in the inset for better visibility. Statistical errors are less than the solid-circle marker size.

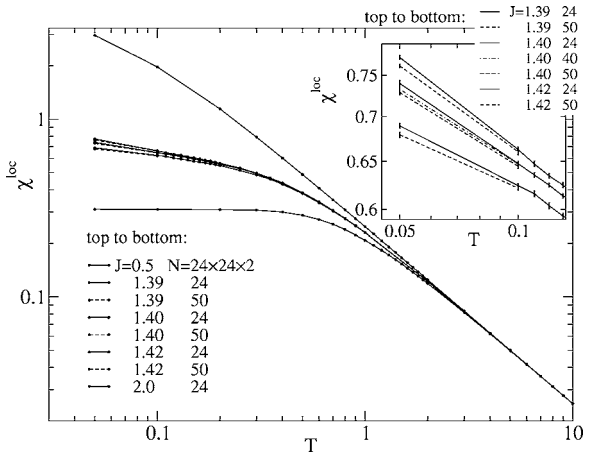

FIG. 5. Impurity susceptibility χ^{loc} vs temperature. Solid line with solid circle markers: $L=24$ for $0.05\leqslant T\leqslant 10$ and $0.5\leqslant J\leqslant 2.0$. Dashed line with solid circle markers: $L=50$ for $0.05\leqslant T\leqslant 0.1$ and $1.39\leqslant J\leqslant 1.42$. Inset: low-$T$ region including additional results for $L=40$ at $J=1.40$ (dashed-dotted). Legends refer to lines from top to bottom. Statistical errors are less than the solid-circle marker size in the main panel and are indicated by bars in the inset. In the quantum critical regime χ^{loc} displays a cross-over region with power-law behavior $\chi^{loc}\approx cT^{-\alpha}$ with $\alpha\approx 0.20(5)$.

fits to a scale-free behavior of the form $\chi_u\approx a+bT^c$ with $c\approx 1.25$. However, this exponent differs from that obtained in the NLσM, i.e., $c=1$.[20,21] Assuming the SKN to be of the same universality class than the NLσM we are forced to treat the curvature in Fig. 3 as deviations from scaling present already at rather low temperature. As is shown in Fig. 3, a reasonable description of the QMC results can be obtained including a second order nonuniversal contribution. This behavior should be contrasted against the AFM bilayer Heisenberg model, where critical linear T scaling has been found in a comparable temperature range.[23] At the QCP χ_u vanishes for $T\to 0$ due to the opening of the spin gap and for $J>J_c$ exponential behavior should replace the scaling. Vanishing of the offset a at $J_c=1.40(1)$ in Fig. 3 is consistent with J_c as from the static structure factor.

For the sake of consistency it is interesting to consider the uniform susceptibility χ_u also as a function of J in the low-temperature limit $T\ll J$. On approaching the QCP from the LRO side one expects χ_u to vanish due to the incipient spin gap. The corresponding QMC results are shown in Fig. 4. Extracting J_c from this figure is less straightforward, both due to the sizeable temperature variation and to the lack of a scaling prescription for χ_u as $J\to J_c$. Nevertheless, as can be seen in the inset, a value of $J\approx 1.4$ for the QCP is consistent with the suppression of χ_u.

Now we turn to the individual impurity-spins longitudinal susceptibility

$$\chi^{loc}=\int_0^\beta d\tau\langle T_\tau S_{Il}^z(\tau)S_{Il}^z\rangle \tag{7}$$

where l refers to a particular site, say $l=0$ within the Kondo spin layer I. Figure 5 shows a log-log plot of χ^{loc} vs T for $0.05\leqslant T\leqslant 10$ and $0.5\leqslant J\leqslant 2$. At $J=0$ χ^{loc} obeys Curie's law. For $J\neq 0$ but $J<J_c$, we expect χ^{loc} to saturate at some cross-over temperature $T^\star\lesssim J$ due to the coupling of the impurity spin to the planar moments within the AFM LRO state. In agreement with this, Fig. 5 signals a departure from $\chi^{loc}\propto T^{-1}$ for $T\approx 0.2$ at $J=0.5$, i.e., in the AFM LRO state. Similarly, for $J>J_c$ we expect a Pauli-like saturation of χ^{loc} for $T\leqslant T^\star$ with $T^\star\lesssim J$ due to the local dimer formation between the impurity spins and the planar sites. This can also be seen in Fig. 5 for $J=2$. The interesting point of Fig. 5, however, is that it suggests a crossover from the high-temperature Curie behavior to a region of power-law behavior $\chi^{loc}\propto T^{-\alpha}$ with an exponent α different from unity in the vicinity of the QCP. Future QMC analysis should focus on additional data in the thermodynamic limit at $T<0.05$ to elaborate on this observation. From Fig. 5 we extract $\alpha\approx 0.20(5)$ at $J=1.40$. The error on this exponent is rather large, due to the error in determining the QCP and due to the temperature range of only one decade to fit to. Regarding finite-site effects, the situation for χ^{loc} is similar to that for χ_u. As shown in the inset of Fig. 5, in the vicinity of the QCP the thermodynamic limit is reached for $L\gtrsim 24(50)$ if $T\gtrsim 0.1(0.05)$. Similar effects are expected at the lowest temperature $T=0.05$ for $J=0.5$ and 2.0 and have not been considered.

Finally, we analyze the temperature dependence of the ratio of the total staggered structure factor to the total staggered susceptibility of Eq. (5). This is shown in Fig. 6 for $0.05\leqslant T\leqslant 10$ and $0.5\leqslant J\leqslant 2$. Nonlinear error propagation of the QMC data through Eq. (5) leads to substantially larger statistical errors on R as compared to the remaining quantities evaluated in this work. Several properties of R can be realized based on general grounds. First, for $T\gg\max\{J,1\}$, i.e., in the *classical regime*, $\chi_A(\mathbf{q})=S_A(\mathbf{q})/T$ for any wave vector $\mathbf{q}$ and therefore $R\to 1$. This behavior of R is obeyed for all values of J displayed in Fig. 6. Next, we note that the zero-temperature limit of the ratio $S_A(\mathbf{Q})/\chi_A(\mathbf{Q})$ will be a T-independent constant whenever the system has no LRO at the wave vector $\mathbf{Q}$ and is gapped. This is true for any finite system, where $S_A(\mathbf{Q})$ and $\chi_A(\mathbf{Q})$ will both saturate at finite values as $T\to 0$. It is also true in the thermodynamic limit

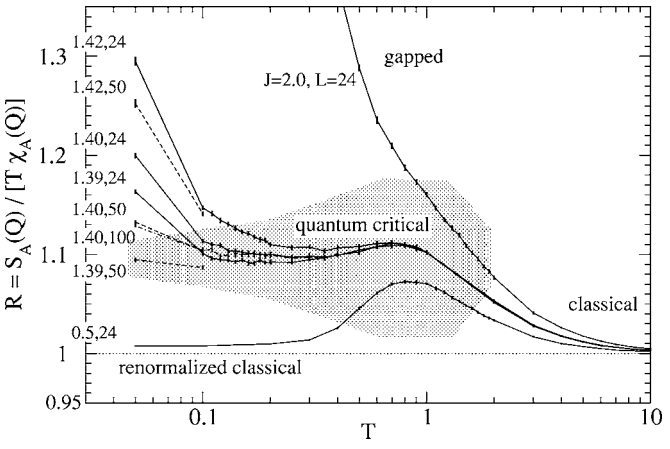

FIG. 6. Solid (dashed) [dashed-dotted]: ratio R of the total staggered structure factor and susceptibility vs temperature for $0.5 \leqslant J \leqslant 2.0$ and $L=24(50)$ [100]. In the classical (renormalized classical) regime, i.e., $T \to \infty$ ($T \to 0$, $J < J_c$), R is expected to be 1. In the gapped state $R \propto 1/T$ as $T \to 0$. In the quantum critical regime, roughly sketched by the shaded region, R differs from unity, however approaching a constant as $T \to 0$. Size of statistical errors is given by vertical bars.

where $S_A(\mathbf{Q})$ and $\chi_A(\mathbf{Q})$ will both be exponentially activated to leading order. Therefore, $R \propto 1/T$ in the thermodynamic limit in the *quantum disordered* regime, i.e., for $J > J_c$, which is consistent with the increase of R in Fig. 6 for $J=2$. In addition to this, $R \propto 1/T$ for any other value of J below a characteristic temperature set by finite size gaps. This is particularly obvious for $J \approx J_c$ where strong finite size effects occur for $T < 0.1$. This effect also sets the magnitude of R for $J \approx J_c$ in Fig. 1. Finally, in the AFM LRO phase the system allows for a classical description in terms of the order parameter modes leading to a *renormalized classical regime* for which $R(T \to 0) = 1$ again.[20,21] This is consistent with the behavior for $J=0.5$ in Fig. 6 and with R in Fig. 1. From a comparison of R at fixed T and identical J in panels (a) and (c) of the latter figure one can also deduce that the small difference between R and unity in the renormalized classical regime decreases upon increase of L. Lowering the temperature from the classical to the renormalized classical regime, one crosses the *quantum critical regime* in which $R > 1$ due to quantum fluctuations.[21,22] For $J < J_c$ this regime has a finite extend in temperature only. Close to the QCP, however, i.e., for $J=1.4$ and 1.39, Fig. 6 strongly suggests that R approaches a temperature independent constant $R \approx 1.10(1)$ as $T \to 0$. Analysis of the NLσM has resulted in $R=1.09$.[21,22] In turn, the quantum critical regime starts at $T \sim 1$ and extends down to $T=0$ at the QCP. Unfortunately, in this regime, R is is very sensitive to the system size. This will be the issue of future QMC studies.[18]

Fruitful discussions with E. Dagotto and the kind hospitality of the National High Magnetic Field Laboratory at Florida State University in the early stages of this project are gratefully acknowledged. A comment by M. Vojta on the scaling analysis is appreciated. Part of this work has been supported by DFG Grant No. BR 1084/1-3.

[1] S. Sachdev, Rev. Mod. Phys. **75**, 913 (2003).
[2] L. Alff, Y. Krockenberger, B. Welter, M. Schonecke, R. Gross, D. Manske, and M. Nalto, Nature (London) **422**, 698 (2003).
[3] D. Bitko, T. F. Rosenbaum, and G. Aeppli, Phys. Rev. Lett. **77**, 940 (1996).
[4] C. Rüegg, N. Cavadini, A. Furrer, H.-U. Güdel, K. Krämer, H. Mutka, A. Wildes, K. Habicht, and P. Vorderwisch, Nature (London) **423**, 62 (2003).
[5] A. Schröder, G. Aeppli, R. Coldea, M. Adams, O. Stockert, H. Löhneysen, E. Bucher, R. Ramazashvili, and P. Coleman, Nature (London) **407**, 351 (2000).
[6] Q. Si, S. Rabello, K. Ingersent, and J. L. Smith, Nature (London) **413**, 804 (2001).
[7] S. Doniach, Physica B & C **91**, 231 (1977).
[8] S. Nishigori, H. Goshima, T. Suzuki, T. Fujita, G. Nakamoto, T. Takabatake, H. Fujii, and J. Sakurai, Physica B **186–188**, 406 (1993).
[9] M. Kyogaku, Y. Kitaoka, K. Asayama, T. Takabatake, and H. Fujii, J. Phys. Soc. Jpn. **61**, 43 (1992).
[10] The Rudermann-Kittel-Kasuya-Yoshida interaction $j_{RKKY} \sim J^2/t$ drives LRO at weak-coupling $U/t \to 0$.
[11] M. Feldbacher, C. Jurecka, F. F. Assaad, and W. Brenig, Phys. Rev. B **66**, 045103 (2002).
[12] C. Jurecka and W. Brenig, Phys. Rev. B **64**, 092406 (2001).
[13] Y. Matsushita, M. P. Gelfand, and C. Ishii, J. Phys. Soc. Jpn. **66**, 3648 (1997).
[14] V. N. Kotov, O. Sushkov, Z. Weihong, and J. Oitmaa, Phys. Rev. Lett. **80**, 5790 (1998).
[15] For bond-operator mean-field theory of a $U(1)$-symmetric variant of Eq. (2) yielding $J_c \sim 1.43$ see Ref. 24.
[16] A. W. Sandvik, Phys. Rev. B **59**, R14157 (1999).
[17] O. F. Syljuasen and A. W. Sandvik, Phys. Rev. E **66**, 046701 (2002).
[18] W. Brenig (unpublished).
[19] Bond-operator mean-field theory of the $U(1)$-symmetric Kondo-necklace in Ref. 24 has resulted in $J_c \simeq 1.43$.
[20] S. Chakravarty, B. I. Halperin, and D. R. Nelson, Phys. Rev. B **39**, 2344 (1989).
[21] A. V. Chubukov, S. Sachdev, and J. Ye, Phys. Rev. B **49**, 11919 (1994).
[22] A. Sokol, R. L. Glenister, and R. R. P. Singh, Phys. Rev. Lett. **72**, 1549 (1994).
[23] P. V. Shevchenko, A. W. Sandvik, and O. P. Sushkov, Phys. Rev. B **61**, 3475 (2000).
[24] G.-M. Zhang, Q. Gu, and L. Yu, Phys. Rev. B **62**, 69 (2000).